Journal of
Ceramic Science
and Technology

J. Ceram. Sci. Tech., 07 [04] 365-378 (2016)
DOI: 10.4416/JCST2016-00047
available online at: http://www.ceramic-science.com

Higher Electronics Circuit Integrations within the Fractal Electronics Frontiers

V.V. Mitic*[1, 2], V. Paunovic[1], Lj. Kocic[1]

[1]University of Niš, Faculty of Electronic Engineering, Niš, Serbia
[2]Institute of Technical Sciences of SASA, Belgrade, Serbia

received July 15, 2016; received in revised form November 21, 2016; accepted November 24, 2016

Abstract

Knowledge of the morphology of ceramic grains and pores facilitates understanding of the sintering process. The real intergrain contact surfaces, as highly irregular objects, can only be adequately described by using fractal models. Both micro- and nanostructured shapes of grains and intergranular contacts can be easily reconstructed by using fractal analysis/modeling. Several variations of Coble's two-sphere model are reviewed in this paper. Further, the intergranular capacity model has been reexamined from the perspective of intergranular fractal formations. The area of grains' surface is calculated using fractal correction and fractal dimension. This results in a more precise numerical interpretation of the parameters and related properties of electronic ceramics. In particular, the role of the dielectric constant, being correlated with the fractal nature of intergranular morphology, causes corrections to the Heywang model and Curie-Weiss law. In order to obtain an equivalent circuit model, an intergranular contacts model is determined and implemented for characterization of the electrical properties of barium titanate. The improved material prognosis electronic properties can be given on the basis of micro-/nanostructure fractal relations. Considering the obtained results, new frontiers are established for deeper and higher level of microelectronic integration of electronic circuits, which practically results in a new framework for fractal electronics.

Keywords: Ceramics, Coble's model, Heywang model, Curie-Weiss law

I. Introduction

The sintering process is characterized by extreme complexity due to the simultaneous and successive actions of elementary mechanisms. Generally speaking, it is very difficult to follow all the actions going on and provide a qualitative or quantitative description of these [1–9]. Ceramic grain contacts are essential for understanding the complex electrodynamic properties of sintered materials. The microstructures of sintered $BaTiO_3$ ceramics, observed with the SEM method, are characteristic examples of complex shape geometry that cannot be easily described or modeled. So, one possible approach to describing contact phenomena is the establishment of grain contact models. Detailed research into the intergranular contacts of $BaTiO_3$ ceramics intergranular contacts has shown that they have the greatest influence on electrical properties of the entire sample [3,4]. The intergranular contacts are formed during the sintering process. When two particles of barium-titanate powder to be sintered form a contact, interatomic forces start forming a particle neck in the contact area. When the powder aggregate is sintered and the necks between powder particles are formed, the aggregate may increase in density. Transport mechanisms contribute to the neck growth and densification. A common driving force is the reduction in the surface area and, thus, the reduction of surface free energy of the system. Throughout the process, the neck begins to grow and this process is controlled by various diffusion mechanisms (lattice diffusion, grain boundary diffusion, etc.) with the rates determined by the total flux of atoms arriving at the neck. The objective of this paper is to review the models [10–23] of three or more spherical grains in contact, as the basis for calculation of the values of possible contact areas in a given geometry configuration. This approach proceeds in two directions. First, the neck growth in the time domain is simulated by combining results for contact surface values with the kinetics of forming three or more contact areas. Second, the model of three or more grains in contact is used for establishing an equivalent electrical model of such a grain association. It is shown that a $BaTiO_3$ ceramic sample can be modeled as the impedance containing two capacitors, an inductor and a resistor [7]. As the ceramic sample consists of numerous grains organized in clusters of different sizes, it could be supposed that each cluster and even each intergranular contact within the cluster exhibits similar behavior. The dominant contribution to the equivalent impedance within a wide frequency range comes from the capacitance [7]. So, any intergranular contact can be observed as an intergranular microcapacitor. Based on these considerations, equivalent electrical models of the three- and four-grain clusters are presented. All these models and electrical contact surface processes are based on the application of computer modeling and simulation methods.

* Corresponding author: vmitic.d2480@gmail.com

The extreme complexity of the sintering process necessitates the study of this process on the basis of different sintering models. Most of the sintering models have used the two-sphere model as the simplest model for studying elementary mechanisms responsible for the progress of the sintering process. Such an idealization of the geometry of the sintering particles enables very detailed study of physical processes acting in the contact area. In this paper, Coble's two sphere model [1] is used as a basis for developing a new two-ellipsoid model. The ellipsoidal geometry gives a more appropriate representation of an average grain then the spherical one. The relations connecting geometric parameters of the ellipsoidal model to consolidation parameters – sintering time and temperature – are reformulated. For better understanding of intergranular processes, Coble's model was further generalized for other possible geometric shapes (sphere-polyhedron, polyhedron-polyhedron). Then, the results of a new model are compared to those obtained from Coble's two-sphere model. All calculations are valid for the initial stage of the sintering process.

In consideration of the important role of the fractal geometry interaction, in the domain of intergranular contacts morphology, a wide investigation front was opened to establish the following crucial facts: What is a measure of fractality of ceramic grain contacts? How does this fractality influence microelectronics mechanisms? What is the resulting energetic balance? (since a part of energy is spent on fractal obstacles), etc. Finally, the equivalent impedance intergranular models are considered.

II. The Sphere-Sphere Model

In order to explain the contact between two grains during a sintering process and better understand the electrical properties of $BaTiO_3$ ceramics, we shall start off with Coble's model [1], Fig. 1. In the process of the diffusion in initial-stage sintering, two grains, approximated by spheres, penetrate each other slightly. The volume that fills the intersection of the spheres (the distance between the centers is smaller than the sum of the two radii) transforms into a neck (a kind of the collar circumscribing the contact area), with the following assumptions: (i) x << a, (ii) the volume conservation, (iii) the center-to-center approach, and (iv) the straight-line neck geometry. For the model system topology shown in Fig. 1 [24], the following equations were derived from the volume conservation principle in the contact area:

$$\varrho_1 = \frac{X_2^2}{4R_1}, \quad \varrho_2 = \frac{X_2^2}{4R_2}, \quad X_2 = \sqrt{2}X_1, \tag{1}$$

where ϱ_1, ϱ_2 are the spherical cap heights (forming the common volume of the spheres' intersection), X_1 is the radius of the common circle, X_2 is the radius of the neck formed by diffusion in the initial stage of sintering, R_1 and R_2 are the radii of the two spheres.

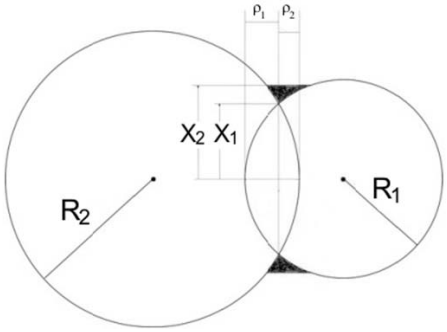

Fig. 1: Coble's two-sphere model.

In the general case, the time-dependent neck radius can be written in the form, $X_2 = g(t;\ T,\ \mathbf{A})$ where T is the sintering temperature, and **A** is the vector of the system parameters

$$\mathbf{A} = \{a,\ \mathbf{D},\ \mathbf{Q},\ \gamma,\ T_m,\ \Omega,\ \delta_B\}$$

where a is the particle radius, **D** and **Q** are the vectors of diffusion coefficients and activation energies of transport mechanisms, respectively, γ the boundary free energy, T_m themelting temperature, Ω the atom volume, and δ_B the effective grain boundary thickness.

Densification and neck formation are the results of the actions of two possible transport mechanisms [6]:

1. Lattice diffusion from the grain boundary,
2. Grain boundary diffusion,
3. Viscous flow (from the grain's bulk),
4. Grain surface diffusion,
5. Grain surface evaporation,
6. Gas diffusion;

It is known that the polyhedral crystal, in equilibrium with the surroundings, would assume a shape with the minimum surface free energy [3]. This principle was translated into the following extended proportion [4], known as the "equilibrium form":

$$\frac{\gamma_i}{r_i} = \frac{kT}{2v_i}\ln\frac{P}{P_\infty}, \quad i = 1,\ 2,\ 3,...$$

where γ_i is the specific surface energy of the *i-th* face of the polyhedral crystal, r_i is the central distance to the *i-th* face, v_i is the molecular volume of the solid, P is the vapor pressure of the polyhedral crystal, and P_∞ is the vapor pressure of a crystal of infinite dimensions.

In their extended model, the same authors also gave the equations for the lattice and boundary diffusion of the following type:

$$Y_1 + Y_2 = \left[B_L t\left(\frac{1}{R_1} + \frac{1}{R_2}\right)\right]^{1/2}, \quad B_L = 8D_L\frac{\gamma\Omega}{kT} \tag{2}$$

$$Y_1 + Y_2 = \left[B_B t\left(\frac{1}{R_1} + \frac{1}{R_2}\right)\right]^{1/3}, \quad B_B = 12D_B\delta_B\frac{\gamma\Omega}{kT} \tag{3}$$

where D_L and D_B are the lattice and grain-boundary diffusion coefficients, respectively.

Equations (2) and (3) are fundamental in modeling the "geometry" of intergrain sintering and the neck forma-

tion. Two spheres with radii R_1 and R_2, the common intersection circle area is given by

$$P_c = \pi\left(R_1^2 - \frac{(d^2 + R_1^2 - R_2^2)^2}{4d^2}\right)$$

provided d is the centers' distance. The common volume is

$$V_C = \frac{\pi}{6}\left(3X_1^2\left(R_1 + R_2\right) + R_1^3 + R_2^3\right)$$

The next step towards a more realistic Coble model is to consider the neck profile update as shown in Fig. 2. The cross-section with the rotation symmetry plane reveals the radius r external neck border rather than a linear segment. In the case $R_1 = R_2$, the graphical interpretation of the cross-section of the common lens-like zone, the "neck" and the relative position of both are shown in Fig. 3 (left side), while on the right side, all mentioned elements are shown in a 3D – perspective projection.

On the other hand, Fig. 4 displays the functional dependence of $r(R, h)$, where R is the radius of spheres (which are equal), and h is the thickness of half a lens.

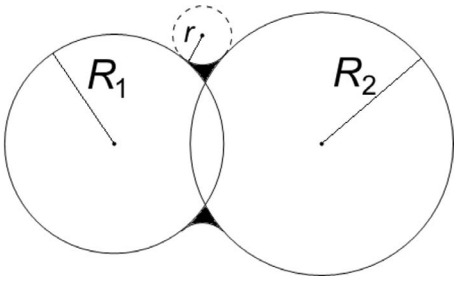

Fig. 2: The "realistic" two-sphere model..

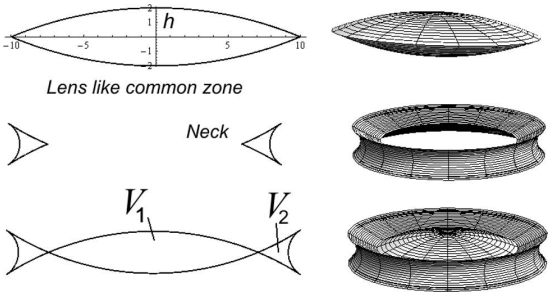

Fig. 3: Planar sections and 3D elements of the "realistic" two-sphere model.

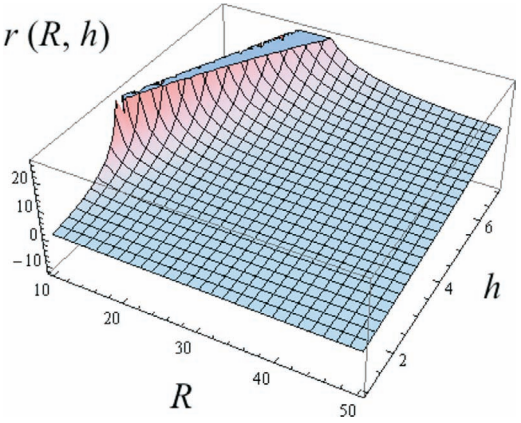

Fig. 4: The radius r from Fig. 3 as a function of $R = R_1 = R_2$, and h, the height of a "half length" of a lens-like common zone.

III. Spherical to Ellipsoidal Model Transformation

The spherical model can be successfully converted into the ellipsoidal one by applying an affine transformation Φ:S $\rightarrow$ E of the form

$$\Phi: \begin{bmatrix} x \\ y \\ z \end{bmatrix} \rightarrow \begin{bmatrix} x/a \\ y/b \\ z/c \end{bmatrix}, \qquad (a, b, c > 0) \tag{4}$$

where a, b and c are scaling parameters introduced in order to generate the ellipsoidal semi-axes a_i, b_i and c_i ($i = 1,2$), and x, y and z are local variables. The main properties of this transformation are its *non-singularity* ($a, b, c \neq 0$) and *continuity* which induces *topological invariance*. This means that the ratio-conserving property of the transformation (4) is of essential importance for the derivation of the ellipsoidal model.

Ellipsoid-ellipsoid model

The grains of the $BaTiO_3$ ceramic sample can be approximated by ellipsoids scattered throughout the material's volume. These ellipsoids can be seen as a model of grains in contact. Actually, owing to sintering pressure and the sintering process, one grain partly penetrates into another, forming a small contact area that can be pretty accurately approximated by the intersection of ellipsoids E_1 and E_2. Our aim is to determine the value of this area as the function of the center distance of the grains δ_E^0 (Fig. 5).

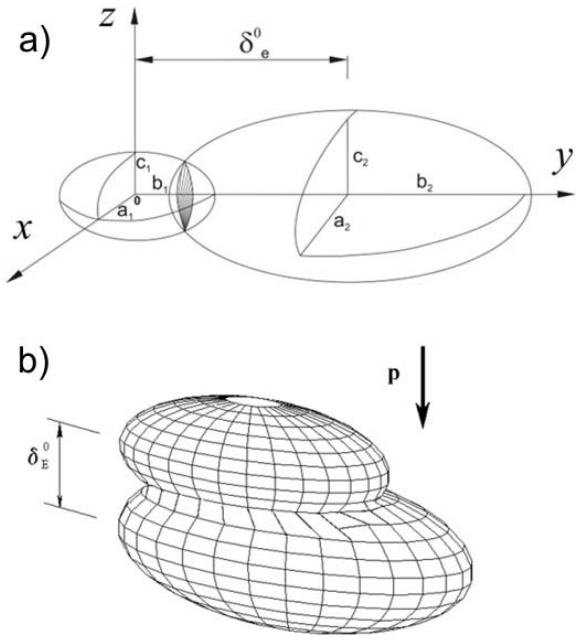

Fig. 5: a) Ellipsoidal grain approximation, b) neck growth of two ellipsoidal grains in the sintering process.

Assuming that the ellipsoidal axes are pairwise parallel and lengths of the axes are proportional by the factor k, two ellipsoids E_1 and E_2, having centers at $C_1 = (x_1, y_1, z_1)$ and $C_2 = (x_2, y_2, z_2)$ from [3], being coaxial (having parallel axes) with semi-axes a_i, b_i, c_i ($i = 1, 2$) provided that $a_i > b_i > c_i$, and $a_2/a_1 = b_2/b_1 = c_2/c_1 = k$ ($k > 0$), are considered (Fig. 5a). Suppose that E_1 and E_2 approximate two neighboring grains in the sintered $BaTiO_3$ ceramics (Fig. 5b).

A straightforward calculation indicates that the distance between C_1 and C_2 at the beginning of sintering (sintering time = 0) is given by

$$\delta_E^o = \frac{1+k}{\sqrt{\frac{\cos^2\alpha}{a_1^2}+\frac{\cos^2\beta}{b_1^2}+\frac{\cos^2\gamma}{c_1^2}}}$$

where ($\cos\alpha$, $\cos\beta$, $\cos\gamma$) is the unit vector of C_1C_2-segment. The difference between the grain center distances at the beginning and at the end of the sintering process during the elapsed time $\delta(\tau)$ is given by

$$\delta(\tau) = \delta_E^o - \delta_E(\tau) = \left[1+\frac{X_2^2}{4kR_1^2}\right]\delta_E^o$$

The value of $\delta(\tau)$ contains information about dynamics of the intergrain neck formation. From this formula, we can derive the neck radius via the proportionality factor k as

$$X_2 = \sqrt{4\cdot R_1^2\cdot k\cdot\left(\frac{\delta_E\cdot\sqrt{\frac{\cos^2\alpha}{a^2}+\frac{\cos^2\beta}{b^2}+\frac{\cos^2\gamma}{c^2}}}{1+k}-1\right)}$$

where R_1 is the radius of the spherical grain corresponding to ellipsoidal grain E_1.

IV. The Modeling Procedure

For modeling of spherical grains the polyhedron-polyhedron model system is used.

The approximated ellipsoidal surface of a grain is represented by series of interconnected adjacent polygons with C^0 continuity [13] (Fig. 6).

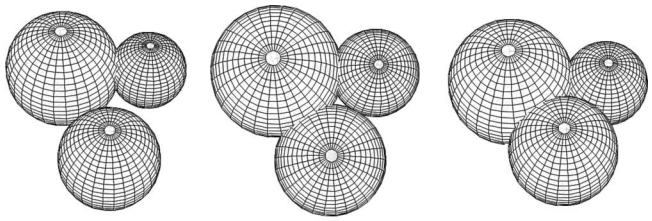

a. **b.** **c.**

Fig. 6: 3D model of three spherical grains in contact during **a.** initial, **b.** middle and **c.** final moment of simulation.

Also, the belonging function is used for the representation of the grain. It is the real function $f(x, y, z)$ representing the grain as follows: an arbitrary point $M(x_1, y_1, z_1)$ belongs to the interior of grain if $f(x_1, y_1, z_1) \geq 0$, and it is out of grain if $f(x_1, y_1, z_1) < 0$.

Two grains are fixed in space so that they can touch or intersect each other, and the third one is approached along the determined direction. We have observed the process from the moment of contact between a mobile grain and one of the static grains until the moment of the assimilation of the grains – the pore between them disappears.

In course of the simulation, the area of each contact surface, the distance between each pair of grains as well as the length of the pore formed between grains have been calculated.

The edge polygons were not considered owing to their insignificant influence on the value of the total area (less than 10^{-4} for the approximation of a grain with 10^6 polygons) as well as the considerable impact on the simulation rate.

V. Ellipsoidal Contact Model

To the best of the author's knowledge, all known intergrain contact models of sintered ceramics use the spherical approximations of grains. Contrary to this, the observations based on a review of the SEM photographs lead to the conclusion that majority of the $BaTiO_3$ ceramic grains can be better approximated by ellipsoids than by spheres. So, it is interesting to consider a pair of grains in contact as two ellipsoids partly penetrating each other. In this way, we can extend those elements of Coble's model concerning the contact zone area [14].

Consider two ellipsoids E_1 and E_2, having centers at $C_1 = (x_1, y_1, z_1)$ and $C_2 = (x_2, y_2, z_2)$ from [3], being coaxial (having parallel axes) with semi-axes a_i, b_i, c_i (i = 1, 2) provided that $a_1 > b_1 > c_1$, and $a_2/a_1 = b_2/b_1 = c_2/c_1 = k$ ($k>0$). And suppose that E_1 and E_2 approximate two neighboring grains in the sintered $BaTiO_3$-ceramics, so that $E_1 \cap E_2 = (x_p, y_p, z_p)$. A straightforward calculation indicates that the distance δ_E^0 between C_1 and C_2 in the beginning of sintering (sintering time $\tau = 0$) is given above.

By the formula (1) $X_2 = \sqrt{2}X_1$, where X_1 is given by

$$X_1 = \sqrt{\frac{R_1^2+R_2^2}{2}-\frac{d^2}{4}-\frac{\left(R_1^2-R_2^2\right)^2}{4d^2}}, \qquad R_2 \leq d \leq R_1+R_2,$$

where d is a distance between the centers of the spheres and $R_2 \geq R_1$. If we denote $q = R_1/R_2$ then the neck radius will be given by

$$X_2(s) = R_2\sqrt{1+q^2-\frac{(s-1)^2}{2q^2}-\frac{q^2(q^2-1)}{2(s-1)^2}}, \qquad (5)$$

where $s = (d - R_2)/R_1$. Formula (5) gives the relationship between the neck radius and distance of the spheres' centers d normalized to the unit interval. The corresponding diagram is given in Fig. 7.

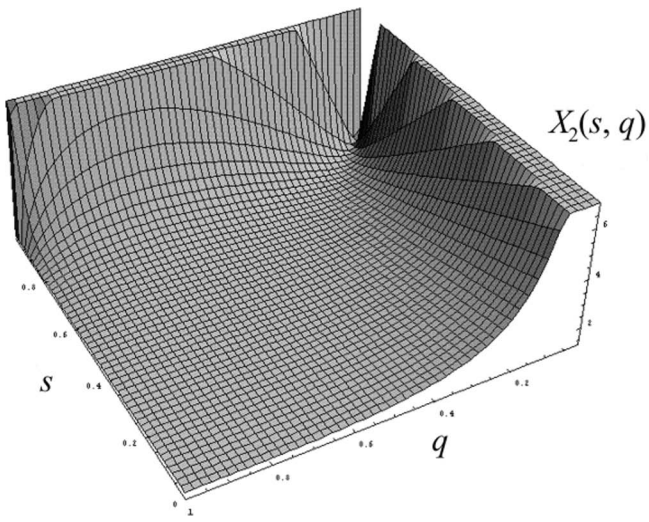

Fig. 7: Diagram of X_2 via $(d - R_2)/R_1$ and q.

VI. Sphere-Polyhedron Model

Suppose that a ceramic grain has an approximately spherical shape but the roughness of the surface justifies replacing the spherical model with the polyhedral one. For the sake of describing a constructive method of obtaining such a polyhedron, we will consider a specific subdivision procedure, which is illustrated in Fig. 8. A sphere is replaced by a regular polyhedron inscribed in the sphere. Among the five regular polyhedra, icosahedron is a good choice for two reasons. First, it is the best approximation of the sphere; second, all its faces are triangles which simplifies the subdivision procedure [6, 17].

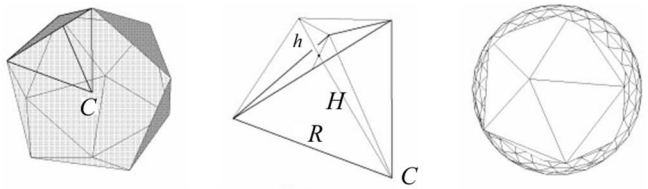

Fig. 8: Icosahedron subdivision geometry.

Consider two grains, one approximated by an n-stage polyhedron (inscribed into a sphere having radius R_1), another by a sphere (radius = R_2). Suppose that these two spheres penetrate each other as in Fig. 2, for the same spacing $\varrho_1 = \varrho_2 = \varrho$, and consequently the same common circle radius $X_1 = X_2 = X$. Now, we need to evaluate the volume of the "cap" of n-stage polyhedron contained within the R_2 - sphere. For this purpose, we will use the cubic function that indicates the increase in the volume of the cap with the height ϱ and cap circle radius X: $V_{cap} = \mu\varrho(3X^2 + \varrho^2)/6$. After n subdivision iterations, an approximate formula for the common volume value reads [17]

$$(V_n)_{cap} = \frac{3 \cdot V_n}{R_1^3} \cdot \varrho^2 \cdot \left(R_1 - \frac{\varrho}{3} \right) \qquad (6)$$

where $V_n = V_0 \left[1 + k + k\beta \cdot \frac{1 - (k\beta)^{n-1}}{1 - k\beta} \right]$ is a polyhedron volume after n-steps, $\beta = \frac{\alpha}{1 + k\alpha}$ and $\alpha = \frac{4 \cdot \pi \cdot (3 - \sqrt{5}) - 5}{5 \cdot k} - 1$.

During the initial sintering process stage, two grains penetrate each other and form a neck. The diameter of the neck is determined by the volume conservation law.

VII. Polyhedron - Polyhedron Model

Aside from a sphere, a ceramic grain can be approximated by a polyhedron. The typical approach uses the intersection of an *octahedron* O, and a *cube* C (Fig. 9) in a way that the vertices of the octahedron are the cube's side centers. In this case, the *octahedron* is fully inscribed in the cube (Fig. 9, leftmost), and $O \cap C = O$. Also, the octahedron O can be considered as having its original size, or $\lambda \times O$, with $\lambda = 1$. If the multiplication factor increases up to 1.35, the intersection becomes a *truncated octahedron* (Fig. 9, middle). For $\lambda = 1{,}5$, the *cuboctahedron* is obtained as an intersection (Fig. 9, right). Further increasing λ yields a *truncated cube* and finally the *cube*.

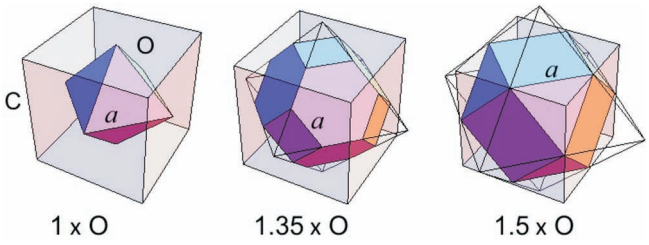

Fig. 9: Grain's approximations by the octahedron-cube intersection.

The main geometric parameter influencing the energetic behavior of the grain is the area-volume ratio, A/V. Providing the side length of each polyhedron is a, the A/V ratio is given in Table 1.

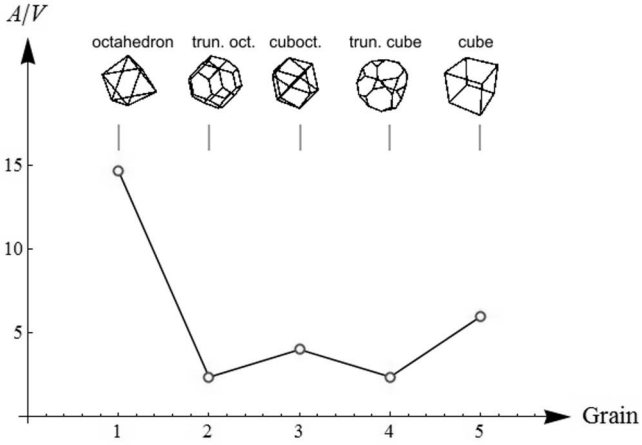

Fig. 10: Different grain approximations.

The diagram integrating the data from Table 1 is given in Fig. 10.

Table 1: Octahedron-cube intersection A/V ratio.

	A	V	A/V	$\sim A/V$ for $a = 1$
octahedron	$\sqrt{3}a^2$	$\sqrt{2}a^3/12$	$6\sqrt{6}/a$	14.6969
truncated octahedron	$\left(6 + 12\sqrt{3}\right) a^2$	$8\sqrt{2}a^3$	$\frac{3\sqrt{2}\left(1 + 2\sqrt{3}\right)}{8a}$	2.36745
cuboctahedron	$\left(6 + 2\sqrt{3}\right) a^2$	$\frac{5}{3}\sqrt{2}a^3$	$\frac{3\sqrt{2}\left(3 + \sqrt{3}\right)}{5a}$	4.01528
truncated cube	$2\left(6 + 6\sqrt{2} + \sqrt{3}\right) a^2$	$\frac{1}{3}\left(21 + 14\sqrt{2}\right) a^3$	$\frac{6}{7}\left(3 - 2\sqrt{2}\right)\left(6 + 6\sqrt{2} + \sqrt{3}\right)$	2.38496
cube	$6a^2$	a^3	6	6

The importance of this model is having a simple tool for the manipulation and fast evaluation whenever it is necessary to process a huge number of grains. It can also be used as a starting point for developing the fractal model of intergrain configuration. Here, we start with two polyhedra, P_m and P_n obtained as an m - stage or n - stage output of the procedure described above (Fig. 10). So, we can use formula (5) with R_1 and R_2 as the corresponding radii of the circumscribed spheres. The neck radius value is dependent on the parameters V_n, R_1, R_2, ϱ, k, α and β. With this procedure, the geometry of two polyhedral grains in contact can be successfully solved.

VIII. The Heywang Model and the Curie-Weiss Law

The most widely accepted model to explain PTCR effect is the Heywang model [25], which describes the resistance-temperature behavior based on a double Schottky barrier. This barrier is caused by deep acceptor states trapped on the grain surface. The height of the barrier at the grain boundaries is described as:

$$\phi_0(T) = \frac{e n_S^2}{8\varepsilon_0 \varepsilon_{gb}(T) N_D} \tag{7}$$

where N_s is the acceptor state density; N_d is the charge carrier density; T is the temperature; ε_o is the permittivity of free space, and ε_r is the relative permittivity of the grain boundary region.

Thus the resistivity R is given by:

$$\rho_S = R_0 \exp\frac{e\phi_0}{kT} \tag{8}$$

where R_0 is a constant, k is the Boltzmann constant, and e is the electron charge. According to the Curie-Weiss Law [26]:

$$\varepsilon_r = C/(T - T_c) \tag{9}$$

where C is the Curie-Weiss constant, T is the temperature, and T_c is the Curie temperature. Above the Curie point, the resistivity increases quickly because of the variation of ε_r. Thus, the PTCR effect is directly related to the grain boundary. According to Eq. 1, N_s, N_d, and ε_r can greatly affect the height of the barrier. As will be indicated further on, all above formulas (7), (8) and (9) are amenable to corrections due to the presence of the fractal nature component within the ceramics microstructure.

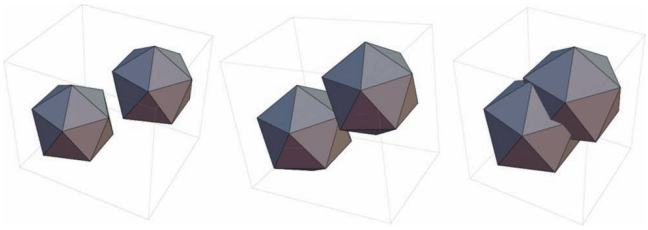

Fig. 11: Ceramic grains approximated by polyhedra in the sintering process.

IX. Temperature Impact

Arguing about the crystal surface's "natural roughness" as a collection of macroscopic steps on the arbitrary section surface of the crystal plane section, Frenkel [27] put forward that this roughness does not coincide with the crystal faces' atomic roughness, with small surface energy, which can occur as the consequence of thermal fluctuations at high temperatures. This temperature consideration illustrates the impact on dynamic processes within the ceramic body. Such impact generates a motion inside the ceramic crystals in the Fermi gas form, containing different particles such as electrons (Bloch wave), atoms, atomic nuclei, etc. [28]. In essence, this motion has a Brownian character and necessitates the introduction of the third fractality factor – the factor of movements, α_M ($0 < \alpha_M < 1$). Our hypothesis [29] is that the working temperature of $BaTiO_3$ ceramics must be influenced by these three fractality factors, correcting the "theoretic" temperature as

$$T_f = \alpha T, \tag{10}$$

where α is a fractal corrective factor. As will be shown below, α is composed of three "sub-factors": the already mentioned α_M as well as the other two, designated α_s and α_p, the role of which will be further explained in more detail in the last section titled "Inner fractality and α-corrections". The functional relationship will be expressed as

$$\alpha = \Phi(\alpha_s, \alpha_P, \alpha_M) \tag{11}$$

The argument for this expectation resides in the fact that the geometrically irregular motion of numerous particles has to release the extra energy into the system. In other words, the fractality of the system represented by the three factors α_s, α_p, and α_M should increase the overall energy of the system, and this increment must be subtracted from the input energy which is in fact an input thermal energy denoted by T. In other words, $T_f = T - \Delta T$ and since it follows from (10) that

$$\alpha = \frac{T_f}{T} = \frac{T - \Delta T}{T},$$

it gives $0 < \alpha = 1 - \Delta T/T < 1$.

The nature of the function in (11) is currently unknown, but at the first moment, the linear approximation will suffice,

$$\Phi(\alpha_s, \alpha_P, \alpha_M) = u\alpha_s + v\alpha_P + w\alpha_M,$$

where $u, v, w < 0$ are real coefficients satisfying $u + v + w = 1$.

If we reconsider formula (9), it gives us a hint of alpha correction embodied in the corrective coefficient α_0. On the other hand, in formula (10) there is another corrective coefficient, this time correcting the temperature. To find a connection between α_0 and α, the Curie-Weiss law should be considered, giving temperature dependence of the dielectric constants of $BaTiO_3$ ceramic grain's contact zone

$$\varepsilon_r(T) = \frac{C_c}{T - T_S} \tag{12}$$

where T_s is the Curie temperature and C_c is the Curie constant. If ε_r is corrected to gain the value $\alpha_0\varepsilon_r$, then from (10) and (12) it follows $\alpha_0\varepsilon_r = C_c/(\alpha T - T_s)$. After the elimination of the Curie constant C_c using (12), the following is obtained:

$$\alpha = \frac{1}{\alpha_0} + \left(1 - \frac{1}{\alpha_0}\right)\frac{T_C}{T}, \text{and reversely, } \alpha_0 = \frac{T - T_C}{\alpha T - T_C}, \qquad (13)$$

which are the formulas and α_0 with temperature T. Fig. 12 visualizes the relationship between α and α_0, where the natural range for both α and α_0, are deliberately extended for better insight.

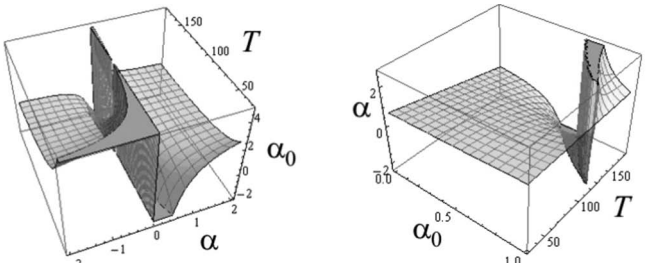

Fig. 12: The dependence of α on T and α_0 according to (13).

More generally, every expression that contains a function of temperature, say $F(T)$, if it is differentiable, may be expanded to the Taylor series as

$$F(\alpha T) = F(T - \Delta T) = \sum_{k=0}^{+\infty} \frac{1}{k!} F^{(k)}(T)(-1)^k \Delta T^k$$

Hence, there are many important formulas associated with the Heywang model containing temperature as the main variable.

X. Intergranular Impedance Model

Taking into account that the intergrain contact surface is the area where processes, in the electro-ceramic material's structural complex grain-contact-grain, occur at the electronic level, it can be presented as an electrical equivalent network consisting of three *RC* branches as noted in the introduction (Fig. 13).

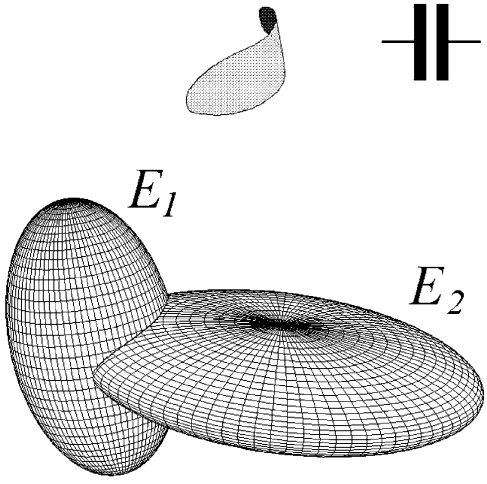

Fig. 13: Equivalent electrical model of contacted grains.

All this allowed us to consider the $BaTiO_3$ ceramic sample as a system with a huge number of mutually contacted grains forming clusters. For each of them, it is possible to establish the equivalent electrical model and, for defined set of input parameters, using symbolic analysis, obtain the frequency diagram. However, the simple *RC* is not sufficient to explain the resonant behavior of a ceramic sample. In order to calculate the equivalent impedance for a wide frequency range, the equivalent electrical circuit for a ceramic material can be introduced as an equivalent impedance Z_e, containing two capacitances C and C_e, an inductance L and a resistance R. Therefore it is more likely that the equivalent circuit model of contacted grains has parallel and series branches as presented in Fig. 14.

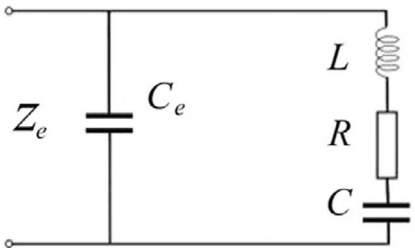

Fig. 14: Two grains in contact forming a microcapacitor.

Two grains (Fig. 13), partly penetrating each other, and the corresponding microcapacitor model, formed by the contact area is shown therein. This area has a fractal structure, which means that an effective size of S is greater than if it was smooth. A striking example of Le Méhauté *et al.* concerning lithium batteries is given in Mandelbrot [10]. For this reason, we will focus our next section on methods that can help identify the type of fractal typical of $BaTiO_3$ ceramics.

Now, consider an intergranular contact impedance as shown in Fig. 14. Here, C_e is the main capacity component while C, R and L are parasitic capacitance, resistance and inductance respectively, without α-correction, which means that intergranular geometry is considered as being flat. It is not difficult to see that the equivalent impedance, with α-correction included should be

$$Z_e = \frac{1 + \alpha_0 (C R s + C L s^2)}{\alpha_0 (C_e + C) s + \alpha_0^2 C_e C (R + L s) s^2}, \quad s = j\omega = j2\pi f,$$

or, expressed via frequency

$$Z_e = \sqrt{\frac{A^2}{4\pi f^2 B^2} + \frac{\alpha_0^4 C^4 R^2}{D^2}}$$

where

$$A = 4\pi^2 \alpha_0^2 C^2 f^2 (4\pi^2 \alpha_0 C_e f^2 L^2 + \alpha_0 C_e R^2 - L) - 8\pi^2 \alpha_0^2 C C_e f^2 L + \alpha_0 v C + \alpha_0 C_e,$$
$$B = \alpha_0 C^2 (4\pi^2 \alpha_0 C_e^2 f^2 (4\pi^2 f^2 L^2 + R^2) - 8\pi^2 \alpha_0 C_e f^2 L + 1) + 2\alpha^2 C C_e (1 - 4\pi^2 \alpha_0 C_e f^2 L) + \alpha^2 C_e^2,$$
$$D = 4\pi^2 \alpha_0^4 C^2 C_e^2 f^2 R^2 + (\alpha_0 C (4\pi^2 \alpha_0 C_e f^2 L - 1) - \alpha_0 C_e)^2.$$

In this manner, except for C_e, C, L, R and f, Z_e also includes the corrective factor α_0 and, thus, it also depends on α as is evident from the graphs in Fig. 15.

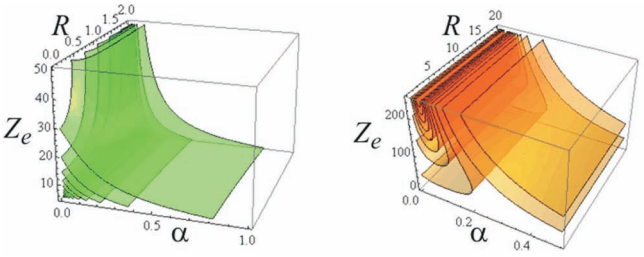

Fig. 15: The level surfaces of intergranular impendence Z_e given by (9) as a function of $0 < \alpha < 1$, $0 < R < 2$, T =80 °C and f = 1(8)80 and for c_e = 0.1; c = 0.01; L = 0.001 (left); c_e = 0.01; R = 1; L = 0.001 (right); Physical units are neglected.

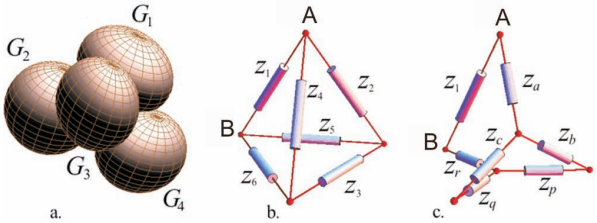

Fig. 16: a. Four grains of $BaTiO_3$ ceramics approximated by ellipsoids. b. Tetrahedral configuration of associated intergranular impedances. c. After triangle-to-star transformation.

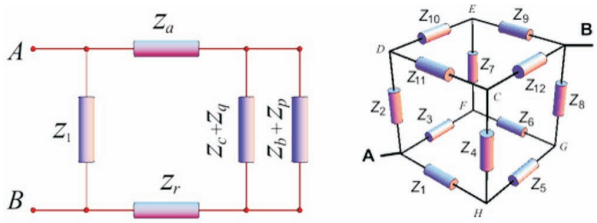

Fig. 17: Left. The equivalent circuit for the four-grain contacts. Right. Cube of impedances.

If more than two grains are in contact, and this is the most common case in the bulk of ceramics, the situation becomes much more complicated. Let the simple case of four grains in contact be considered (Fig. 16a). If these grains have four contacts, then the configuration of intergranular impedances will have the form of a tetrahedron (Fig. 16b). The equivalent impedance between the grains G_1 and G_4 is the same as between the points A and B on the tetrahedral scheme. The triangles $Z_2Z_3Z_4$ and $Z_3Z_5Z_6$ can be transformed into the corresponding "stars" $Z_aZ_bZ_c$ and $Z_pZ_qZ_r$ (Fig. 16c) with

$$Z_a = \frac{Z_2Z_4}{\Sigma'},\ Z_b = \frac{Z_2Z_3}{\Sigma'},\ Z_c = \frac{Z_3Z_4}{\Sigma'},$$
$$Z_p = \frac{Z_3Z_5}{\Sigma''},\ Z_q = \frac{Z_3Z_6}{\Sigma''},\ Z_r = \frac{Z_5Z_6}{\Sigma''}, \qquad (14)$$

where $\Sigma' = Z_1 + Z_2 + Z_3$ and $\Sigma'' = Z_3 + Z_5 + Z_6$. The equivalent circuit is shown in Fig. 17, and the final calculation gives

$$Z_{AB} = \frac{Z_1(Z_a + Z_b)}{Z_1 + Z_a + Z_b} + \frac{(Z_b + Z_p)(Z_c + Z_q)}{Z_b + Z_c + Z_p + Z_q},$$

or, taking into account (14),

$$Z_{AB} = \frac{Z_1Z_2(Z_3+Z_4)}{Z_1(Z_1+Z_2+Z_3)+Z_2(Z_3+Z_4)} + \frac{Z_3(Z_6(Z_1+Z_2)+Z_3(Z_4+Z_6)+Z_4(Z_5+Z_6))(Z_5(Z_1+Z_3)+Z_2(Z_3+2Z_5+Z_6))}{(Z_1+Z_2+Z_3)(Z_3+Z_5+Z_6)((Z_1+Z_4)(Z_5+Z_6)+Z_3(Z_4+Z_5+Z_6)+Z_2(Z_3+2(Z_5+Z_6)))}. \qquad (15)$$

Suppose all impedances are equal to some Z. Then, according to (15), $Z_{AB} = \frac{5}{3}Z$. If the parasite components L, R and C are neglected, and if $1/Z_i = j\omega\alpha_0C_e = j2\pi f\,\alpha_0C_e$, all i, then

$$Z_{AB} = \frac{5}{3}\frac{1}{j\omega\,\alpha_0C_e} = \frac{1}{j\omega(3\alpha_0C_e/5)}$$

This formula reveals that the overall capacity in the case of tetrahedral configuration is smaller than the single-contact capacity, $C_{AB} = (3/5)\alpha_0C_e$.

Similar calculations in the case of eight grains in contact, arranged in a cubic manner (Fig. 17, right), gives

$$Z_{AB(CUBE)} = \frac{5}{6}\frac{1}{j\omega\,\alpha_0C_e} = \frac{1}{j\omega(6\alpha_0C_e/5)}$$

and therefore, $C_{AB} = (6/5)\alpha_0C_e$, so the capacity of the cubic cluster is larger than the capacity of a single contact.

XI. Combined Grain Approximations

In some cases, a polyhedral approximation is acceptable, as well. In this case a polyhedron can be constructed as a 3D graph the nodes of which are points on the ellipsoidal surface. So, we can consider an approximate model of a group of two grains in three ways: 1. ellipsoid - ellipsoid (EE) contact; 2. ellipsoid - polyhedron (EP) and 3. ellipsoid - grain (EG) contact (Fig. 18).

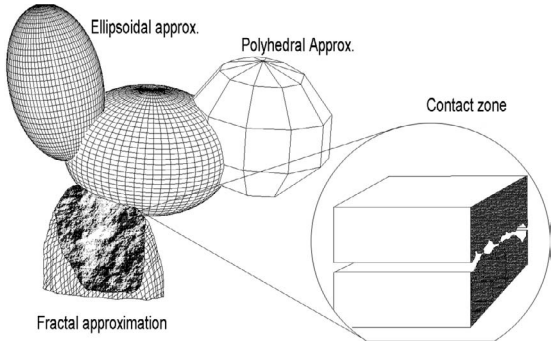

Fig. 18: EE-EP-EG-group of $BaTiO_3$ ceramics grains and a fractal structure of the contact zone.

Here, it is interesting to determine what the distribution of the intergranular contacts looks like and, secondly, what is a more general formula for evaluating the size of all contact patches in the volume unit of $BaTiO_3$ ceramics, and the last, but the most complex, is the question of the nature of intergrain layers and their relationship with microcapacitor distribution. Of course, it must be kept in mind that all the parameters mentioned are the functions of sintering process parameters (t, p and τ).

In the light of the geometric method explained above, we can extend this approach from the case of ee intersections to the case of ep and eg intersections. In fact, the value of the contact area of two grains area is given by $A = \int_s d\sigma$ where S is a mathematical surface that will be described soon and $d\sigma$ is a usual differential element of the surface. For all three models, a surface S can be characterized in the unique way based on the intersection of the ellipsoidal surface with: 1. Another ellipsoidal surface, 2. A polyhedron surface and 3. A real grain surface that can be expressed in terms of fractal functions. Even in the case that the analytical method could be applied (EE), there is no use for this because the method of the evaluation of the above integral must be a numerical one. Consequently, it is reasonable for the method of two surface intersection to be numerical, as well. In all cases, it is sufficient to find discrete points lying along the intersection line. In the case of EE intersection, the analytical solution of the intersection is to be discretized, which reduces the problem in the case of EP intersection. The method is, as follows.

A polyhedron P can be regarded as a union of vertices V and sides σ. The set of vertices is divided by ellipsoidal surface E into two groups: V_1 - vertices inside of E including the surface; V_2 - vertices lying outside of E. These two groups of vertices divide the set of sides into three groups: $\sigma = \sigma_1 \cap \sigma_2 \cap \sigma_3$, where σ_1 are sides with their two endpoints in E, σ_3 are sides outside of E and σ_2 contains all sides that connect vertices from V_1 and vertices from V_2. Each side from σ_2 contains a unique point being characterized by the unique parameter t, $t \in (0, 1)$, so that $(1\text{-}t)\mathbf{p}_1 + t\,\mathbf{p}_2$ is a point on the ellipsoid. If the ellipsoid has semi-axes **a**, **b**, **c** and $\mathbf{p}_1 = (x_1, y_1, z_1)$, $\mathbf{p}_2 = (x_2, y_2, z_2)$, parameter t must obey the quadratic equation $At^2 + Bt + C = 0$, where

$$A = (x_1 - x_2)^2 / a^2 + (y_1 - y_2)^2 / b^2 + (z_1 - z_2)^2 / c^2,$$
$$B = 2\times\left[(x_1 x_2 - x_1^2)/a^2 + (y_1 y_2 - y_1^2)/b^2 + (z_1 z_2 - z_1^2)/c^2\right],$$
$$C = x_1^2/a^2 + y_1^2/b^2 + z_1^2/c^2 - 1.$$

What we want to get is the value of the size of a part of the surface of P that is immersed into ellipsoid [10]. Let this surface be denoted by π, then $|\pi|$ – the value we want – can be approximated by the union of triangular elements. The size of each triangle is given by 1/2 of the modulus of the vector product of its sides.

As far as the EG contact is concerned, the calculation is a little bit complex mainly due to the fact that a fractal grain is defined by recursive functions (a fractal structure of such a contact is shown in magnified detail in Fig. 18). But using the binary tree algorithm and a convex hull property of fractal algorithms, the intersection of one meridian line in fractal grain with an ellipsoid is not difficult to find. Actually, let S_0 be a starting set in 3D space for the recursive procedure of making auto composition of the Hutchinson contractive operator. Then, a sequence of sets has been produced. Being a union of smaller copies of the attractorlet from the previous stage, the new attractorlet obeys the convex hull property, enabling the pinpointing of its intersection within any compact set in 3D. Once the fractal intersection contour is determined, its area can be estimated using the suitable numerical method.

A surface S that appears in the integral formula is the union of all intergrain contact surfaces in a prescribed volume V of the $BaTiO_3$ ceramic sample. This surface can be defined using the characteristic function of some set A

$$\chi_A(x) = \begin{cases} 1, & x \in A \\ 0, & otherwise \end{cases}$$

Let G be a contact zone between any two grains. Define the following function

$$F(x, y, z) = \chi_G(\boldsymbol{r}), \quad \boldsymbol{r} = [x \quad y \quad z]^T \in \boldsymbol{R^3}.$$

It is clear that F is a discontinued function defined over the volume of the sample being considered. Let ∇F be the usual gradient of the function F with the convention that in the point of discontinuity $\boldsymbol{r}_0$, where the line of pre-gradient fraction goes into infinity, it will be taken $\nabla F(\boldsymbol{r}_0) = +\infty$. It is easy to see that the set defined by $\partial G = \{\boldsymbol{r} : |\nabla F(\boldsymbol{r})| > 1\}$ represents the surface of A contact zone (see [10]). In order to extend ΔG on all contact surfaces, it is enough to replace the function F defined above with F_1

$$F_1(x, y, z) = \prod_{i \in I} \chi_{Gi}(\boldsymbol{r})$$

where I is a subset of natural numbers broad enough to number all contact zones. The corresponding surface is $S = \partial G_1$ defined by

$$\partial G_1 = \left\{\boldsymbol{r} \;:\; |\nabla F_1(\boldsymbol{r})| > 1\right\}$$

Therefore, the total contact area is given by

$$A = \int_S d\sigma = \int_V \prod_{i \in I} \chi_{Gi}(\boldsymbol{r})\, d\sigma$$

XII. Non-Contact Intergranular Capacities

If two grains are close to each other but not in direct contact, then neighboring crystal surfaces pair up to form micro-capacitors. The polarization effect causes two close grains to have opposite electric charges and each flat facet from the grain's one half interacts with several similar facets of grain's other closest half (Fig. 19).

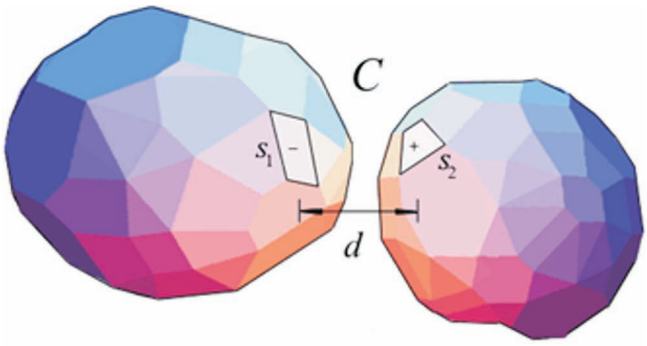

Fig. 19: Two neighboring grains and a micro-capacitor.

Since each facet (S_1 or S_2) belongs to a single plane and no plane contains both facets (if it does, no capacitor exists), then there is a pair of planes intersecting each other forming an acute angle, say φ. Let the distance between centers of the facets be d. In this way kind of "slanted" capacitor is formed. A cross-section showing such a capacitor can be seen in Fig. 20 (left). Note that much of the edge effect of fringing fields should be neglected.

The most appropriate model though is the model of two planes situated as shown in Fig. 20 (right) in a cylindrical coordinate system (ϕ, r, z), where the intersection of planes coincides with z-axes.

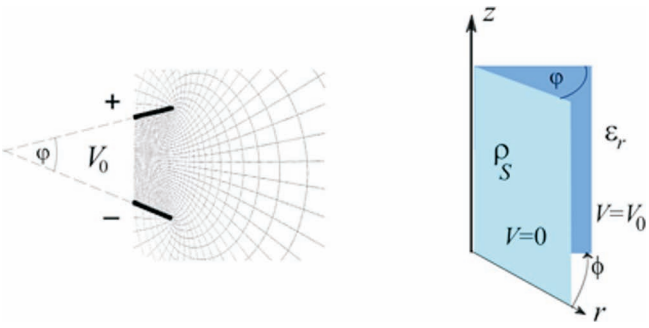

Fig. 20: Electrostatic field configuration for two slanted micro-surfaces and an approximating mathematical model in cylindrical coordinates.

Consider Poisson's equation for electrostatic fields in cylindrical coordinates

$$\frac{1}{r}\frac{\partial}{\partial r}\left(r\frac{\partial V}{\partial r}\right)+\frac{1}{r^2}\frac{\partial^2 V}{\partial \phi^2}+\frac{\partial^2 V}{\partial z^2}=-\frac{\varrho_V}{\varepsilon} \tag{16}$$

with boundary conditions $\phi = 0$, $V = 0$, $\phi = \varphi$, $V = V_0$;

Assuming the geometry of two nonparallel planes, we see that potential V has to be constant along radial and axial coordinates r and z, which implies $\frac{\partial V}{\partial r}=\frac{\partial V}{\partial z}=0$. That simplifies (16) to the partial differential equation

$$\frac{1}{r^2}\frac{\partial^2 V}{\partial \phi^2}=-\frac{\varrho_V}{\varepsilon} \tag{17}$$

The solution of (17) is

$$V=-\frac{1}{2}\frac{\varrho_V}{\varepsilon}r^2\phi^2+c_1\phi+c_2 \tag{18}$$

where c_1 and c_2 are constants regarding the angular coordinate. From the boundary conditions, one gets $c_2 = 0$, and $c_1=\frac{V_0}{\alpha}+\frac{1}{2}\frac{\varrho_V}{\varepsilon}\varphi r^2$, which, being substituted in (18), gives

$$V=\frac{1}{\varphi}V_0\,\phi+\frac{1}{2}\frac{\varrho_V}{\varepsilon}r^2\phi(\varphi-\phi) \tag{19}$$

Of course, $\varepsilon=\varepsilon_0\varepsilon_r$, as it is known $\varepsilon_0 = 8.85\times10^{-12}\,F/m$.

Since $\mathbf{E}=\Delta V$, and since the gradient in cylindrical coordinates evaluates as

$$\operatorname{grad} V(\phi, r, z)=\frac{1}{r}\frac{\partial V}{\partial \phi}\mathbf{e}_\phi+\frac{\partial V}{\partial r}\mathbf{e}_r+\frac{\partial V}{\partial z}\mathbf{e}_z$$

from which one has

$$\mathbf{E}=\frac{1}{r}\frac{\partial V}{\partial \phi}\mathbf{e}_\phi+\frac{\partial V}{\partial r}\mathbf{e}_r=\left(\frac{V_0}{\alpha}\frac{1}{r}+\frac{1}{2}\frac{\varrho_V}{\varepsilon}r(\varphi-2\phi)\right)\mathbf{e}_\phi+\frac{\varrho_V}{\varepsilon}r(\varphi-\phi)\phi\,\mathbf{e}_r$$

Now, the electric flux density $\mathbf{D}=\varepsilon\mathbf{E}$ is then

$$\mathbf{D}=\left(\varepsilon\frac{V_0}{\alpha}\frac{1}{r}+\frac{\varrho_V}{2}r(\varphi-2\phi)\right)\mathbf{e}_\phi+\varrho_V r(\varphi-\phi)\phi\,\mathbf{e}_r$$

where

$$Q=\iint_S D_\phi\,ds=\int_0^{\Delta z}dz\int_R^{R+\Delta r}\left(\varepsilon\frac{V_0}{\alpha}\frac{1}{r}+\frac{\varrho_V}{2}r(\varphi-2\phi)\Big|_{\phi=0}\right)r\,dr=$$

$$=\Delta z\left(\varepsilon\frac{V_0}{\alpha}\Delta r+\frac{1}{6}\varrho_V\varphi\,\Delta r\,R(2R+\Delta r)\right);$$

The choice of limits for z is made to simplify the expression without the loss of generality. Otherwise, the radial coordinate r depends on the distance of the facet element from the intersection line, and it is taken to be R. Although the surface of the facet is approximated by a rectangular element of the area $\Delta s = \Delta z\,\Delta r$, it follows from the familiar formula

$$C=\frac{Q}{|V_a-V_b|}=\frac{Q}{V_0}$$

and

$$C=\frac{\Delta z\,\Delta r}{V_0}\left(\varepsilon\frac{V_0}{\varphi}+\frac{1}{6}\varrho_V\varphi\,R(2R+\Delta r)\right)$$

XIII. Contact Intergranular Capacities

If two grains are in firm contact, they may form capacitance zones having fractal-shaped electrodes. In fact, the fractal dimensions of the grains' surfaces will be reproduced onto the contact zones, forming capacitor plates with identical fractal dimensions. This situation is shown in Fig. 22.

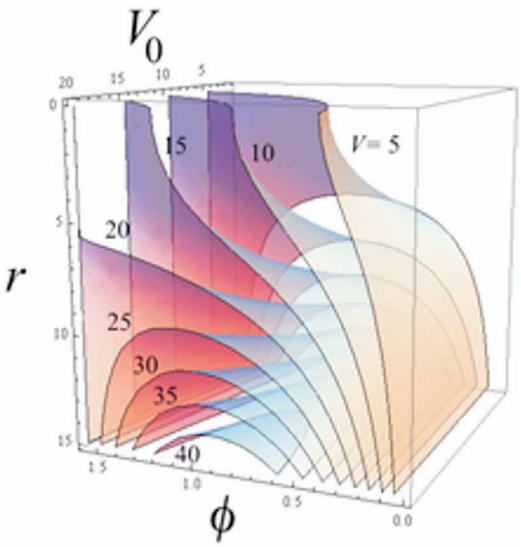

Fig. 21: Solutions (19) of Poisson's equation (2) for voltages 5 to 40 V.

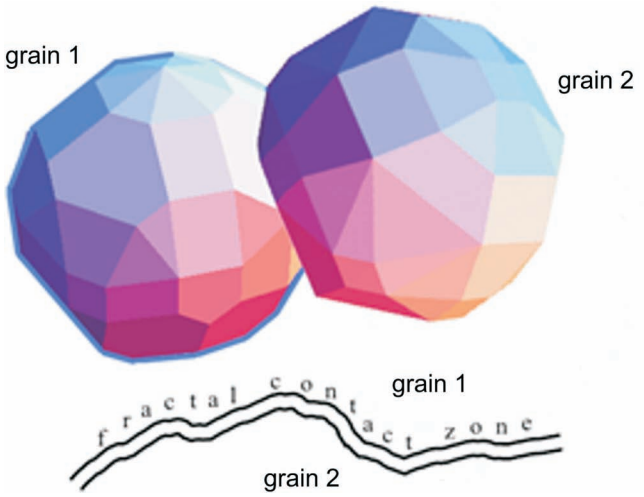

Fig. 22: Contact capacitor zone has fractal morphology.

The contact zone can be approximated by a classic parallel-plates capacitor with distance d and surface area A so that it has the capacity $C_0=\varepsilon\frac{A}{d}$, where ε is the local permittivity constant. Such a capacitor undergoes the fractal transformation using an iterated procedure driven by Iterated Function System $\{w_1, w_2, w_3 \ldots, w_n\}$, where

$$w_k\left(\begin{bmatrix}x\\y\end{bmatrix}\right)=\begin{bmatrix}a_k & 0\\ c_k & d_k\end{bmatrix}\begin{bmatrix}x\\y\end{bmatrix}+\begin{bmatrix}e_k\\f_k\end{bmatrix}=\mathbf{A}_k\begin{bmatrix}x\\y\end{bmatrix}+\mathbf{b}_k$$

is a contractive affine transformation in the plane of the cross-orthogonal section of the capacitor. The values a_k, c_k, d_k, e_k, f_k are determined in such a way corresponding to the adequate form of fractal initiator-generator pair. In the example in the picture, the initiator is the double line,

parallel to each at a distance d, and of length L. The parallel lines are the plates of the capacitor seen from the side. Suppose that the area of the surface is $A = L \times a$, where a is the width of the plates, and that a keeps constant. Then the capacity C_0 has the value

$$C_0 = \varepsilon\, a\, \frac{L}{d}$$

If we set $n = 3$, this means that there are only three contractive mappings. This further means that there are three matrices $\mathbf{A}_1$, $\mathbf{A}_2$, $\mathbf{A}_3$, each of which is "responsible" for mapping the whole double line into the three double segments (Fig. 23). In this manner, each longitude transforms into new values, bounded by the factors of matrix norms

$$\|\mathrm{A}_k\|^2 = \frac{1}{2}\left(a_k^{\,2} + c_k^{\,2} + d_k^{\,2} + \sqrt{\left(a_k^{\,2} + c_k^{\,2} + d_k^{\,2}\right)^2 - 4\, a_k^{\,2} d_k^{\,2}} \right).$$

In other words, the length L of the capacitor will transform into three new lengths: $\|\mathbf{A}_1\|L$, $\|\mathbf{A}_2\|L$, and $\|\mathbf{A}_3\|L$. At the same time, the distance d undergoes the same transformation. In fact, each new capacitor has more or less the same capacity

$$C_1 \cong \varepsilon\, a\, \frac{\|\mathrm{A}_1\|L}{\|\mathrm{A}_1\|d},\ C_2 \cong \varepsilon\, a\, \frac{\|\mathrm{A}_2\|L}{\|\mathrm{A}_2\|d},\ C_3 \cong \varepsilon\, a\, \frac{\|\mathrm{A}_3\|L}{\|\mathrm{A}_3\|d},$$

i.e., $C_1 \cong C_0$, $C_2 \cong C_0$, $C_3 \cong C_0$. Since these capacitors are connected in parallel scheme, the total capacity after the first iteration will be $C^{(1)} \cong 3C_0$. Further iteration will yield 3^2 new capacitors so that we will get $C^{(2)} \cong 3^2 C_0$. Consequently, after N iterations the approximate value of capacity will be $C^{(N)} \cong 3^N C_0$. In the case that the Iterated Function System has n contractive mappings, the whole formula will be $C^{(N,\,n)} \cong n^N C_0$.

To the local fractality embodied in intergranular contacts, the stereological distribution of the contacts throughout the ceramics bulk is to be added. Although these may seem stochastic, it is not so. Some amount of regularity, inherited from a crystallite structure, appears. Some possible basic models are shown in the Fig, 24.

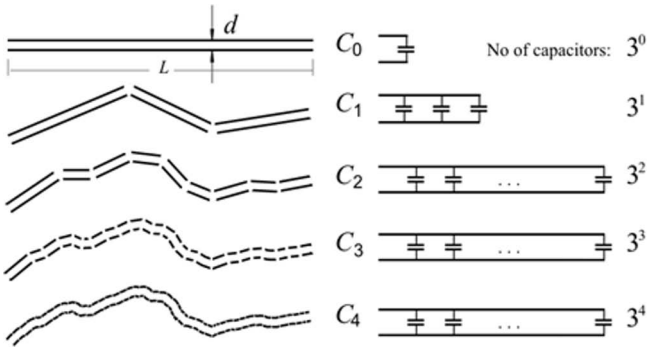

Fig: 23: Modeling intergranular capacitor by Iterated Function Systems and equivalent capacity schemes.

XIV. Inner Fractality and α-Corrections

Note that these fractal dimensions of typical Σ are just slightly above the topological dimensions of the surface, $D_T = 2$. The difference DH_f-$D_T = DH_f$-2 is thereby supposed to be responsible for affection to a part of ferroelectric phenomena in barium titanate ceramics that cannot be explained by purely Euclidean geometry of the grain surfaces. It is convenient to introduce a normalized surface fractality parameter α_S, thus satisfying the inequality

$$(1-\varphi)\min\{DH_f - 2\} < \alpha_S < \varphi \max\{DH_f - 2\}, 0 < \varphi < 1$$

which ensures the unit range

$$0 < \alpha_S < 1$$

Also, $BaTiO_3$ ceramic is a porous material that corresponds to lacunar fractal models. It brings in a new phenomenon. Namely, the solidification of porous and "spongy" materials increases the overall fractal dimension from (theoretically) 2 to full solid 3. In other words, fractal dimension of a porous material, DH_P satisfies $2 < DH_P < 3$. It causes another correction factor $\alpha_P = D_T$ - DH_P, where $D_T = 3$ is dimension of the space and DH_P is corresponding fractal dimension of a porous configuration. Therefore, $0 < \alpha_P < 1$.

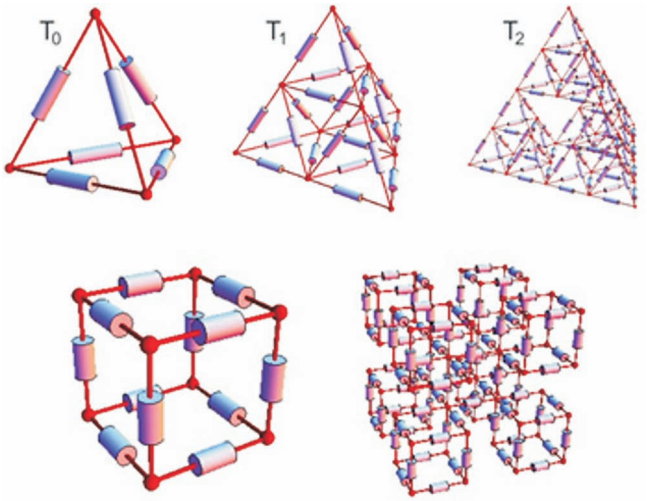

Fig. 24: Possible 3D model of intergranular capacities organized according to the Sierpinski pyramid (top) and Menger sponge (below).

The dimensionless quantities α_S and α_P shall be called "geometric fractality factors". We suggest the existence of the third factor α_M caused by the influence of disorder movement of ferroelectric particles, i.e. the factor of fractal movements.

As it is known, there is a mobile "cloud" of particles in motion within semiconductors (and metals as well) consisting of electrons in atoms with large atomic numbers, nucleons in heavy atomic nuclei, and gases consisting of quasi-particles with half-integral spin. This is called Fermi gas and obeys Fermi-Dirac statistics.

The classic theory of Fermi gas assumes that (i) The interactions between the electrons are irrelevant and can be ignored; (ii) The electrons move in a constant potential and we can ignore everything about the structure of the material; (iii) The crystal comprises a fixed background of N identical positively charged nuclei and N electrons, which can move freely inside the crystal without seeing any of the nuclei (monovalent case); and (vi) Coulomb interactions are negligible because the system is neutral overall.

Now, the real dynamics of the Fermi gas impose the necessity of including the factor of fractal movements α_M, that makes the third factor, next to the geometric ones α_S

and α_P. Since the Fermi gas particles have dynamics similar to the 3D Brownian one, α_M should be a derivate of the Hausdorff fractal dimension DH_M of a Brownian 3D space-filling curve. It is obvious that $1 \le DH_M \le 3$. The lower limit, min $DH_M = 1$, is imposed by the continuity of a particle's trajectory. The upper limit, max $DH_M = 3$, in turn, is the maximum of trajectory complexity in 3D space. It is reasonable to normalize quantity α_M by taking

$$\alpha_M = \frac{1}{2}(DH_M - 1)$$

which gives

$$0 < \alpha_M < 1$$

In this way, three independent dimensionless fractality factors α_s, α_P and α_M are introduced. These are real numbers from the open interval (0, 1).

Now, our hypothesis is that the working temperature of $BaTiO_3$ ceramics must be influenced by these three fractality factors, necessitating correction of the "theoretic" temperature T, to get the new "real" temperature T_f, which is *temperature affected by the inner fractality of the material* $T_f = T - \Delta T$. Obviously, $T_f \le T$ with equality of no fractal structure of S, P or M type is present.

Now, by setting $\alpha = \frac{T_f}{T} = 1 - \frac{\Delta T}{T}$, one has

$$T_f = \alpha T,$$

where α depends on all three alpha-components, so

$$\alpha = \Phi(\alpha_s, \alpha_P, \alpha_M)$$

Now, by the Curie-Weiss law, the relative permittivity will be given by

$$\varepsilon_{r,\alpha} = \frac{C_c}{T_f - T_S} = \frac{C_c}{\alpha T - T_S} = \frac{C_c}{\Phi(\alpha_s, \alpha_P, \alpha_M)\, T - T_S}$$

where C_c is the Curie constant.

So, formula (5) can be modified as follows

$$C = \frac{\Delta z\, \Delta r}{V_0} \left(\varepsilon_{r,\alpha} \frac{V_0}{\varphi} + \frac{1}{6} A_\varphi \varphi\, R(2R + \Delta r) \right)$$

XV. Conclusions

The aim of this paper is to review some intergrain models of the ceramic sintered materials including the generalizations of Coble's two-sphere intergrain contact model. In the initial sintering phase, two grains, approximated by ellipsoids or polyhedrons, form a specific contact zone that is responsible for the dielectric characteristics of $BaTiO_3$ ceramics. In this way, we develop ellipsoid-ellipsoid, sphere-polyhedron and polyhedron-polyhedron models, using the usual Euclidean geometry. In addition, we offer a fractal extension of all those models using the fractal representation of a grain. This representation is obtained as a stochastic subdivision of a regular polyhedron inscribed in a Coble's sphere. The subdivision mechanism is flexible enough to provide possibilities for changing the fractal dimension of the grain – the real number that conveys information on irregularities on the grain's surfaces. The average value of the fractal dimension of $BaTiO_3$ ceramics grains has been estimated in order to accurately reproduce a model of the grain. In the case of the observed models, the normal grain growth is independent of the initial pressing pressure so that the results prove the conjecture that the dielectric constant has a direct correlation with consolidation parameters (pressing pressure, sintering temperature and time). With the simultaneous analysis of the relative dielectric constant, the grain size and the capacitance distribution, optimal intervals for technological parameters – lower sintering temperatures and higher pressing pressures – can be obtained.

Understanding the electrical properties of barium-titanate materials is important for modern device applications and presents a challenge for simulation. In this study, the model of the intergranular impedance is established using the equivalent electrical scheme characterized by a corresponding frequency. According to the microstructures we have obtained for $BaTiO_3$, sometimes doped with rare earth additives, the global impedance of a barium-titanate ceramic sample contains both a resistor and capacity components. The resistor and capacity components were presented as a "sum" of many clusters of micro-resistors and micro-capacitors connected in the tetrahedral lattice. The positions of neighboring grains for the four-grain cluster have been defined and, based on these, the tetrahedral scheme of the mutual electrical influence of $BaTiO_3$ grains has been established. Fractal geometry has been used to describe the complexity of the spatial distribution of $BaTiO_3$ grains. The model of impedances between the clusters of the ceramics grains has been presented and calculations of micro-capacitance generated in the grain contacts of $BaTiO_3$ have been conducted. By controlling the shapes and numbers of contact surfaces on the level of the entire $BaTiO_3$ ceramic sample, the structural properties of this ceramic can be controlled, with the aim of correlation between the material's electronic properties and corresponding microstructure.

High precision of the applied fractal nature mathematics opens up new perspectives for the better evaluation of intergranular capacity as well as the understanding of the spatial distribution of micro-impedances with the further breakthroughs in the field of miniaturization and integration of electronic circuits. With this, we can proceed towards better component and device packing because the possibilities of semiconductor technology are already limited. Presented experimental research and theoretical work is a part of the extended investigations in the area of material structure analysis and the fractal nature domain, which is important for more precise contact surface in the energy storage area and in materials consolidation for battery systems. These results confirm the shapes, grains and reconstruction possibilities of microstructure constituents with the application of Brownian motion particles, through long-term scientific research on the fractal analysis of electronic materials. This is the original contribution to the basic electrochemical thermodynamic parameters area with the introduction of the α, fractal correction function, based on three correction parameters a_S, a_P and a_M, as electrochemistry area functions, especially with regard to energy storage aspects and creating a new approach towards intergranular capacity. This offers a solid base for the future procedure and further application,

in order to create new perspectives and solutions for advanced miniaturization, electronic parameter multi-level integration, materials, components and circuits (especially *C*, *R*, *L*) characteristics as well as better component and electronic circuit packaging.

All of these are of huge importance in many respects. One of these are the new and alternative energy sources. They are also very important with regard to establishing new frontiers in miniaturization. It is a new experimental-theoretical approach framework for a new model line developed by the authors. It could be considered as the electrochemistry area of fractal microelectronics. In this way, we have confirmed the new fractal frontiers in the area of alternative energy sources as a precise and powerful approach.

From the other side, this paper presents a systematic approach towards creating a method for wind motion/turbulences and prediction of influence of a fractal nature. One of the most important wind parameters is fractal analysis of different terrain roughness profiles.

One of the main goals is a contribution to industrial production via the design concept of inventive ideas for final products with best performance. Through this method and results, we are opening up new frontiers and technological processes in fractal microelectronics, especially specific intergranular relations within grain surface coatings. This paves the way towards fractal nature microelectronics of intergranular thin films, and also opens a new "window" towards correlation between "big" and "small", like the roughness of the Earth's relief vs. microscopic microstructures irregularities.

References

1 Coble, R.L.: Effects of particle-size distribution in initial-stage sintering, *J. Am. Ceram. Soc.*, **56**, [9], 461 – 466 (1973)

2 Coble, R.L.: Sintering of crystalline solids. I. Intermediate and final state diffusion models, *J. Appl. Phys*., **32**, 789 – 92, (1961).

3 Gibbs, J.W.: Collected works, Longmans, New York, 1928.

4 Wulff, G.: On the question of the speed of growth and the resolution of crystal surfaces (in German), *Z. Kristallogr*., **34**, 449 – 530, (1901).

5 Mitić, V.V.: Structures and elektrical properties of $BaTiO_3$ ceramics, Begrade: Zadužbina Andrejević (in Serbian), 2001.

6 Kang, S.J.L.: Sintering. Densification, Grain Growth, and Microstructure, Elsevier 2005.

7 DeJonge L., Rahman M.N.: Sintering of Ceramics, Handbook of Advanced Ceramics, S.Sowmya et al. (Eds.), Elsevier (78s), 2003

8 Cho, Y.K., Kang, S.L., Yoon, D.Y.: Dependence of grain growth and grain-boundary structure on the Ba/Ti ratio in $BaTiO_3$, *J. Am. Ceram. Soc.,* **87**, 119 – 124, (2004).

9 Zhang, D., Weng, G., Gong, S., Zhou D.: The kinetics of initial stage in sintering process of $BaTiO_3$ based PTCR ceramics and its computer simulation, *Mater. Sci. Eng. B*, **99**, [1 – 3], 88 – 92, (2003).

10 Mitic, V.V., Paunovic,V., Mancic, D., Kocic, Lj., Zivkovic, Lj., Pavlovic, V.B.: Dielectric properties of $BaTiO_3$ doped with Er_2O_3 and Yb_2O_3 based on intergranular contacts model. In Advances in electroceramic materials, ed. K.M. Nair, D. Suvorov, R.W. Schwartz, and R. Guo, 137 – 144. John Wiley & Sons, Inc. 2009.

11 Mitic, V.V., Pavlovic, V., Paunovic, V., Purenovic, J., Kocic, Lj., Jankovic, S., Antolovic, I., Rancic, D.: Intergranular properties and structural fractal analysis of $BaTiO_3$-ceramics doped by rare earth additives. In: Advanced processing and manufacturing technologies for structural and multifunctional materials V, ed. Tatsuki Ohji, Mrityunjay Singh, Sujanto Widjaja, and Dileep Singh, 121 – 132., 2011

12 Mitrovic, I., Mitic, V.V.: $BaTiO_3$-ceramics electrical model based on intergranular contacts, *J. Eur. Ceram. Soc.*, **21**, [15], 2771 – 2775, (2001).

13 Mitić, V.V., Kocić, Lj. M., Ristić, M.M.: The Fractals and $BaTiO_3$-ceramics sintering, 1997, *Key Eng. Mat.*, **136**, 1060 – 1063, (2001).

14 Mitić, V.V., Petković, P., Kocić, Lj.: $BaTiO_3$-ceramics capacitance in terms of consolidation parameters, Proc. of Micro Materials Conference and Exhibition Micro Mat 97, Berlin, 1103 – 1105, 1997.

15 Mitić,V., Živković, Lj.: Effect of nonstoichiometry on the microstructure and electrical properties of $BaTiO_3$-ceramics, Proc. of the 12th Conference on glass and ceramics, Bulgarian Ceramic Society, Varna, Bulgaria, 479 – 484, 1997.

16 Mitić, V.V., Kocić, Lj. M., Mitrović, I.: $BaTiO_3$-ceramics structure and consolidation process, extended abstracts of the 5th Conference and Exhibition of the European Ceramic Society, Euro Ceramics *V*, Part 2, Versailles, France, 924 – 927, 1997.

17 Mitić, V.V., Kocić, Lj.M., Ristić, M.M.: The fractals and $BaTiO_3$-ceramics structure, extended abstracts of the 5th Conference and Exhibition of the European Ceramic Society, Euro Ceramics V, Part 2, Versailles, France,. 1060 – 1063, 1997.

18 Nikolić, Z.S., Mitrović, I., Mitić, V.V.: Computer simulation of neck growth during sintering process, Proc. of the IX World Round Table Conference on Sintering held in Belgrade: Advanced Science and Technology of Sintering, edited by Stojanović *et al*., Kluwer Academic/Plenum Publishers, New York, pp. 61 – 66, 1999.

19 Mitić, V.V., Kocić, Lj. M., Mitrović, I.Z.: Fractals in ceramic structure, Proc. of the IX World Round Table Conference on Sintering" held in Belgrade:Advanced Science and Technology of Sintering, edited by Stojanović *et al.*, Kluwer Academic/ Plenum Publishers, New York, pp. 397 – 402, 1999.

20 Mitić, V.V., Mitrović, I.Z.: $BaTiO_3$ structure prognosis, Proc. of the IX World Round Table Conference on Sintering held in Belgrade: Advanced Science and Technology of Sintering, edited by Stojanović *et al.*, Kluwer Academic/Plenum Publishers, New York, pp. 431 – 436, 1999.

21 Mitic, V.V., Pavlovic, V.B., Kocic, Lj., Paunovic, V., Mancic, D.: Application of the intergranular impedance model in correlating microstructure and electrical properties of doped $BaTiO_3$, *Sci. Sinter.*, **41**, [3], 247 – 256, (2009).

22 Mitić, V., Paunović, V., Mancic, D., Kocic, Lj.,. Zivković, Lj., Pavlović, V.B.: Dielectric properties of $BaTiO_3$ doped with Er_2O_3, Yb_2O_3 based on intergranular contacts model, *Ceram. Trans.*, **204**, 137 – 144, (2009).

23 Mancic, D., Paunovic, V., Vijatović, M., Stojanović, B. Zivković, Lj., Electrical characterization and impedance response of lanthanum doped barium titanate ceramics, *Science of Sintering*, 40 [3], 283 – 294, (2008).

24 Chen, J.H. Johnson, P.F.: Computer simulation of initial stage sintering in two-dimensional particulate systems, P.E. Russell, Ed., Microbeam Analysis- 405 – 409, 1989,

25 W. Heywang, H. Thomann, Electronic Ceramics, London and New York, 1991.

26 Pontes, F.M., Pontes, D.S.L., Leite, E.R., Longo, E., Chiquito, A.J., Pizani, P.S., Varela, J.A.: Electrical conduction mechanism and phase transition studies using dielectric properties and Raman spectroscopy in ferroelectric $Pb0.76Ca0.24TiO_3$ thin films, *J. App. Phy.,* **94**, [11], 7256. (2003).

27 Frenkel, Y.I.: On the surface crawling particles in crystals and the natural roughness of natural faces, JETP, **16**, [1], (1948).

[28] Mitić, V.V., Fecht, H.J., Kocić,Lj.: Materials science and energy fractal nature new frontiers, Contemporary Materials (Renewable energy sources), VI, 2 (2015), 190 – 203.

[29] Mitić, V.V., Paunović, V., Kocić, Lj.: Fractal approach to $BaTiO_3$-ceramics micro-impedances, *Ceram. Int*., **41 – 5**, 6566 – 657, (2015).

[30] Mandelbrot, B.B., The fractal geometry of nature, W. H. Freeman, New York 1983.

[31] Boyd D.W.: The osculatory packing of a three dimensional sphere, *Canad. J. Math.*, 25, 303 – 322, (1973).

[32] Borkovec M. *et al.*: The fractal dimension of the apollonian sphere packing, *Fractals*, **2**, [4], 521 – 526 (1994).